# PERK-mediated induction of miR-5p and miR-3p arms of miR-616 regulates cell growth by targeting c-MYC

Vahid Arabkari[1, 4†], Afrin Sultana[1†], David Barua[1], Mark Webber[1], Terry Smith[2], Ananya Gupta[3] and Sanjeev Gupta[1*]

[1] Discipline of Pathology, School of Medicine, Clinical Science Institute, Lambe Institute for Translational Research, University of Galway, Galway, Ireland

[2] Molecular Diagnostic Research Group, College of Science, University of Galway, Galway, Ireland

[3] Discipline of Physiology, School of Medicine, University of Galway, Galway, Ireland

[4]Krefting Research Centre, Department of Internal Medicine and Clinical Nutrition, Institute of Medicine, University of Gothenburg, Gothenburg, Sweden

*Corresponding author
Email: sanjeev.gupta@universityofgalway.ie

† These authors contributed equally to work

**Keywords:** unfolded protein response, ER stress, miR-616, c-MYC, breast cancer

# ABSTRACT

C/EBP homologous protein (CHOP), also known as DNA damage-inducible transcript 3 (DDIT3), is a member of CCAAT/enhancer-binding protein (C/EBP) family. The expression of CHOP is upregulated during unfolded protein response (UPR), and sustained CHOP activity plays an important role in UPR-induced apoptosis. MicroRNA-616 is localized in an intron of the CHOP gene. However, regulation of miR-616 expression during UPR and its function in breast cancer is not clearly understood. We show that miR-5p/-3p arms of miR-616 are expressed with levels of 5p arm higher than 3p arm. During conditions of UPR, the expression of miR-5p and miR-3p arms of miR-616 and its host gene (CHOP) was concordantly increased primarily in a PERK-dependent manner. We show that ectopic expression of miR-616 significantly suppressed cell growth and colony formation, whereas knockout of miR-616 increased it. We identified that MYC proto-oncogene (c-MYC) gene is repressed during the UPR and targeted by miR-616. Further, we show that expression of miR-616 and CHOP is downregulated in human breast cancer, where expression of miR-616 was associated with poor overall survival (OS) in luminal A subtype and better OS HER2 subtype of breast cancer. In summary, our results suggest a dual function for the DDIT3 locus, where CHOP protein and miR-616 can co-operate to regulate cancer progression.

57 # INTRODUCTION

58 The endoplasmic reticulum (ER) is a crucial cellular organelle that plays important role in
59 folding and maturation of proteins that transit through the secretory pathway. Stimuli that
60 compromise the protein handling capacity of the ER activate an evolutionarily conserved
61 pathway known as unfolded protein response (UPR). Three major sensor molecules that
62 initiate the UPR are activating transcription factor 6 (ATF6), inositol-requiring enzyme 1α
63 (IRE1) and protein kinase RNA-like endoplasmic reticulum kinase (PERK) (1). During resting
64 state the activity of PERK, IRE1 and ATF6 is kept under control by interaction with ER
65 chaperone glucose-regulated protein 78 (GRP78); however, upon accumulation of misfolded
66 proteins in ER, GRP78 dissociates from these molecules, leading to their activation (2). Upon
67 dissociation with GRP78, IRE1 auto-phosphorylates and oligomerizes leading to the
68 activation of its endoribonuclease domain present in the cytosolic domain. Active IRE1
69 catalyses the unconventional splicing of XBP1 mRNA and regulated IRE1-dependent decay of
70 transcripts (RIDD) (3). While splicing of XBP1 mRNA is an adaptive response to UPR, RIDD
71 has many context dependent outcomes (3). ATF6 is a transmembrane protein located in the
72 ER membrane with an N-terminus cytoplasmic domain containing a DNA-binding motif and
73 a C-terminus ER-luminal domain that interacts with GRP78 (4). During UPR, ATF6 is relocates
74 from the ER to the Golgi compartment. In the Golgi, ATF6 is processed by intramembranous
75 proteolysis causing the release of the transcriptionally active N-terminal cytosolic domain,
76 p50ATF6 (5). During UPR, active PERK phosphorylates eukaryotic initiation factor 2α (eIF2α),
77 causing reduced translation initiation for a majority of cellular proteins and preferential
78 translation of a subset of mRNAs including activating transcription factor 4 (ATF4) (6, 7).
79 Phosphorylation of eIF2α leads to general translational block and preferential translation of

80 a subset of mRNAs including activating transcription factor 4 (ATF4) (7). Phosphorylation of
81 NRF2 by PERK attenuates Keap1-mediated degradation of NRF2 and promotes expression of
82 NRF2-target genes through the antioxidant response elements (ARE) (6). The increased
83 protein handling capacity of the ER and degradation of unfolded proteins induced by UPR
84 attempts to restore the protein homeostasis and increase cell survival. However, if UPR-
85 induced mechanisms fail to alleviate ER stress, UPR activates apoptosis.
86
87 MicroRNAs (miRNAs) are small (~20–23 nucleotide) single-stranded RNA molecules that
88 regulate gene expression in a sequence-specific manner (8). The increased expression of
89 miR-616 has been reported in androgen-independent prostate cancer (9, 10), gastric cancer
90 (11), non-small cell lung cancer (NSCLC) (12), hepatocellular carcinoma (HCC) (13) and
91 gliomas (14). MiR-616 targets tissue factor pathway inhibitor (TFPI-2) in prostate cancer (9);
92 PTEN in HCC and gastric cancer (15); SOX7 in glioma and NSCLC (14). However, miR-616-3p
93 has been reported to reduce XIAP expression and potentiate apoptosis in HUVECs (16).
94 LINC01614 promotes head and neck squamous cell carcinoma progression via PI3K/AKT
95 signalling pathway and miR-616-3p can inhibit cancer progression by downregulating
96 LINC01614 expression (17). Ye et al. reported that miR-616-3p inhibited cell growth and
97 mammosphere formation of breast cancer cells by suppressing GLI1 (18), while Yuan
98 reported that miR-616-3p promoted breast cancer cell migration and invasion by targeting
99 TIMP2 and regulating MMP signalling (19). Overall, these observations suggest that miR-616
100 exhibits both oncogenic and tumour suppressor functions in context- and/or tissue-
101 dependent manner. Additional studies are warranted to further investigate the role of miR-
102 616 in human cancers.
103

104 During the past few years, work from several groups has revealed that all three branches of
105 the UPR regulate specific subsets of miRNAs (20, 21, 22, 23). The modes of regulation
106 include both increase and decrease in expression by UPR-regulated transcription factors
107 such as ATF6, XBP1, ATF4 and NRF2 as well as degradation by RIDD activity. The key feature
108 of UPR-dependent miRNA expression is fine tuning of the ER homeostasis to modulate
109 cellular adaptation to stress and regulation of cell fate. The gene encoding miRNA-616 is
110 located in the second intron of CHOP/DDIT3. This genomic co-location of miR-616 with
111 CHOP/DDIT3 suggests a role for miR-616 in UPR. Indeed, increased expression of miR-616
112 has been reported during conditions of UPR (24, 25). Hiramatsu et al., focused on the
113 expression of miR-616-5p (24) while Arabkari focused on the expression of miR-616-3p (25).
114 Here we have evaluated the expression of both miR-5p/-3p arms of miR-616 as well its host
115 gene (CHOP) during conditions of UPR.
116
117 We show that expression level of miR-616-5p was higher than miR-616-3p in human cancer
118 cells and tissues. During conditions of UPR, the expression of both miR-5p/-3p arms of miR-
119 616 and CHOP was increased in a PERK-dependent manner. Our results show that miR-616
120 regulates cell growth and proliferation along with regulation of c-MYC expression. We
121 identified that MYC proto-oncogene (MYC) gene is repressed during the UPR and targeted
122 by miR-616. Finally, we show that expression of miR-616 and CHOP (host gene of miR-616)
123 is reduced in human breast cancer. In summary, our results suggest that CHOP locus
124 generates two gene products, where CHOP protein and miR-616 can act together to
125 regulate cancer progression.
126

127 # METHODS

128 **Cell culture and treatments** - Human breast cancer cells (MCF7 and BT474) were purchased
129 from ECACC. HCT116 cells were kind gift from Dr. Victor E. Velculescu, Johns Hopkins
130 University, USA. HEK 293T cells were gift from Indiana University National Gene Vector
131 Biorepository. The MCF7, BT474 and HEK 293T cells were maintained in Dulbecco's modified
132 eagle's medium. HCT116 cells were maintained in McCoy's 5A modified. The medium was
133 supplemented with 10% heat inactivated foetal bovine serum (FBS) and 100 U/ml penicillin
134 and 100 µg/ml streptomycin with 5% CO2 at 37°C. Thapsigargin (Cat # 1138) and BFA (Cat #
135 1231) were purchased from Tocris Bioscience. All reagents were purchased from Sigma-
136 Aldrich unless otherwise stated.
137
138 **Plasmid constructs** - miExpressTM precursor miRNA expression clones, miR-CTRL and miR-
139 616 (pEZX-MR03 vector) were sourced from GeneCopoeia, Rockville, MD, USA. The lentiviral
140 plasmids pLV [CRISPR]-hCas9:T2A: Puro-U6>mir-616 expressing hCas9 protein and miR-616
141 targeting gRNA were obtained from VectorBuilder Inc, Chicago, IL, USA. The sequences of
142 two miR-616 targeting gRNAs are 5'-GGAAATAGGAAGTCATTGGA-3' and 5'-
143 GTGTCATGGAAGTCACTGAA-3'. PCDH-Flag-c-MYC was a gift from Hening Lin (Addgene
144 plasmid # 102626; http://n2t.net/addgene:102626; RRID: Addgene_102626).
145
146 **Generation of stable cell lines –** MCF7 cells were transduced with lentiviruses to generate
147 stable miR-616 overexpressing and miR-616 knockout sub-clones. Lentivirus was generated
148 by transfecting lentiviral plasmids along with packaging plasmids in 293T cells using jetPEI
149 transfection reagent as described previously (26).
150

151 **RNA extraction, Reverse transcription reaction and real time quantitative PCR** - Total RNA
152 was isolated using Trizol (Life Technologies) according to the manufacturer's instructions.
153 RPLP0 and GAPDH (for mRNAs) and U6 SnRNA (for miRNAs) were used as a reference genes
154 to determine the relative expression level of target genes between treated and control
155 samples using △△Ct method.
156
157 **Colony formation assay** - The cells were plated in 6 well plates and were grown for 14 days.
158 After 14 days, cells were washed twice with PBS and fixed with 10% formaldehyde for 5
159 minutes and stained with 0.5 % crystal violet for 10 minutes. The number of colonies were
160 counted in five random view fields under a microscope and average number of colonies was
161 determined. Colony size was determined using Image J software.
162
163 **X-CELLigence cell proliferation assay** - xCELLigence experiments were performed using the
164 Real-Time Cell Analyzer (RTCA) Dual Plate (DP) instrument according to the manufacturer's
165 instructions (Agilent.com). Briefly, instrument-specific specially designed gold
166 microelectrodes fused microtiter 16-well cell culture plate (0.2 cm2 well surface area; 250 µl
167 volume per well) was used to monitor the real-time changes expressed as Cell index (CI).
168 Cell Index is defined as (Rn−Rb)/15 where Rn is the cell–electrode impedance of the well
169 with the cells and Rb is the background impedance of the well with the medium alone. The
170 background impedance was measured by adding 50 µl of medium to each well of the E-Plate
171 before seeding the cells. After seeding (2500 cells/well), the E-plate was incubated at room
172 temperature for 30 min and then transferred to the instrument. Cell proliferation was
173 monitored every 15 min for 50 h.
174

175 **Western blot analysis** - Western blotting procedure has been described previously. After
176 blocking with specific solution nitrocellulose membranes were treated with specific primary
177 antibodies including c-MYC (Santa Cruz Biotechnology Cat# sc-40), ERα (Merck Millipore
178 Cat# 2828587) and β-Actin (Sigma, Cat# A-5060) at 4°C for overnight. After washing three
179 times with PBS/0.05%Tween solution, the membranes were incubated with appropriate
180 secondary antibody at room temperature for 2 hours. The membranes were then washed
181 twice with PBS/0.05%Tween and once with PBS and finally the signals were detected using
182 Western Lightening chemiluminescent substrate (Perkin Elmer, Netherlands, Cat
183 #NEL104001EA).
184
185 **Statistical Analysis** - The GraphPad was used for statistical analysis and generating graphs.
186 Two-tailed unpaired t-test was performed to determine statistically significant differences
187 between independent groups. Results with a $p<0.05$ were considered statistically significant.
188

189 # Results

190 ## Expression of miR-616-5p is higher than miR-616-3p

191 Several miRNAs are located within the introns of either protein coding or non-coding genes,
192 and are referred to as intronic miRNAs (27). The genes which harbour these miRNAs are
193 embedded are called host genes. MiR-616 is an intronic miRNA localized in the first intron of
194 DDIT3 gene (**Fig 1A**). Both the 5' and 3' arms of the precursor duplex can generate mature
195 miRNAs, and are referred to as miRNA-5p and -3p (27, 28). The miRBase
196 (http://www.mirbase.org) (29) has discontinued the use of miRNA/miRNA* nomenclature
197 and use of miR-5p and miR-3p nomenclature (30), based solely on 5'- or 3'-arm derivation of

198 the mature miRNA is now recommended. The sequences of mature miR-616, accession
199 numbers and the previous names of miR-616-5p and -3p as per miRNA/miRNA*
200 nomenclature are shown in Fig 1B. Indeed, both 5p and 3p arms of miR-616 have been
201 shown to be expressed in human cancers (11, 31). Next we evaluated the expression of miR-
202 616-5p and miR-616-3p in human cancers. Initially expression of miR-616-5p and miR-616-
203 3p was determined in various human cancer cell lines by qRT-PCR. We observed that
204 endogenous expression of miR-616-5p was higher than miR-616-3p in all the cell lines tested
205 (**Fig 1C**). Next we analysed the expression of miR-616-5p and miR-616-3p in the TCGA
206 dataset from different human cancers using OncomiR (http://www.oncomir.org), a web-
207 based tool for miRNA expression analysis. We observed a higher expression of miR-616-5p
208 as compared to miR-616-3p in all the cancer types evaluated (**Fig 2**). Of note the ratio of
209 miR-616-5p and miR-616-3p expression varied considerably across the different tissue
210 types. These results suggest that both 5p and 3p arms of miR-616 are expressed where miR-
211 616-5p accumulates at higher levels than miR-616-3p but their ratio is controlled in tissue-
212 specific manner.
213

214 **Fig 1. Basal expression of miR-616-5p and miR-616-3p in human cancer cell lines**. (A)
215 Schematic representation of the CHOP locus is shown. The exons are shown in blue and gray
216 line between them represents intron. The miR-616 is located in the first intron. The arrows
217 show the direction of transcription of the gene. The protein coding regions are shown in
218 dark blue and untranslated regions are shown in light blue. (B) The name, accession number
219 and sequence of miR-616-5p and 3p are shown. (C) Total RNA from indicated cells was used
220 to determine the expression of miR-616-5p and miR-616-3p by qRT-PCR and normalised
221 against RNU6. Expression of miR-616-3p in MCF7 cells was arbitrarily set at 1. Error bars
222 represent mean ±S.D. from three independent experiments performed in triplicate. *P <
223 0.05, two-tailed unpaired t-test compared to miR-616-3p in MCF7 cells.
224
225 **Fig 2. Expression of miR-616-5p and miR-616-3p in human cancers**. Web-based algorithm
226 at (http://www.oncomir.org/) was used to assess the expression of miR-616-5p and miR-
227 616-3p. Log2 mean expression of miR-616-5p and 3p in indicated cancer types is shown. (N
228 = number samples in each cancer type). ACC: adrenocortical carcinoma; BLCA: bladder

229 urothelial carcinoma; BRCA: breast invasive carcinoma; CESC: cervical squamous cell
230 carcinoma and endocervical adenocarcinoma; CHOL: cholangiocarcinoma; COAD: colon
231 adenocarcinoma; ESCA: esophageal carcinoma; HNSC: head and neck squamous cell
232 carcinoma; KICH: kidney chromophobe; KIRC: kidney renal clear cell carcinoma; KIRP: kidney
233 renal papillary cell carcinoma; LGG: brain lower grade glioma; LIHC: liver hepatocellular
234 carcinoma; LUAD: lung adenocarcinoma; LUSC: lung squamous cell carcinoma; MESO:
235 mesothelioma; OV: ovarian serous cystadenocarcinoma; PAAD: pancreatic
236 adenocarcinoma; PCPG: pheochromocytoma and paraganglioma; PRAD: prostate
237 adenocarcinoma; READ: rectal adenocarcinoma; SARC: sarcoma; SKCM: skin cutaneous
238 melanoma; STAD: stomach adenocarcinoma; TGCT: testicular germ cell tumours; THCA:
239 thyroid carcinoma; THYM: thymoma; UCEC: uterine corpus endometrial carcinoma; UCS:
240 uterine carcinosarcoma; UVM: uveal melanoma
241
242
243 **Increased expression of miR-616-5p and miR-616-3p during UPR**

244 It was initially proposed that intronic miRNAs are derived from the same primary transcript
245 as their host genes thereby leading to co-expression and co-regulation of miRNA and
246 cognate host gene (27). Analysis of expression of 175 miRNAs and their host genes across
247 twenty four different human organs reported a significantly correlated expression profile
248 (32). Recent evidence however, shows significant discordant expression between intronic
249 miRNAs and host genes. Two likely explanations for this discordant expression are: (i)
250 miRNAs have their own independent promoters and (ii) crosstalk between microprocessor
251 cleavage and mRNA splicing (33, 34)**.** Next, we evaluated the co-regulation of miR-616 and
252 its host gene (CHOP) during conditions of UPR. MCF7, BT474 and HCT116 cells were either
253 treated or untreated with thapsigargin (TG) or Brefeldin A (BFA) for 24 hours and expression
254 of CHOP, miR-616-5p and miR-616-3p was determined. The expression level of CHOP, miR-
255 616-5p and miR-616-3p was upregulated in all three cell lines tested, during ER stress (**Fig.**
256 **3A-C**). Next we investigated the role of ATF6, PERK and IRE1, three key mediators of the UPR
257 in upregulation of miR-616 expression. For this purpose, we used MCF7 control (MCF7
258 PLKO) and knockdown of UPR sensors (MCF7 XBP1-KD, MCF7 PERK-KD and MCF7 ATF6-KD)
259 sub-clones of MCF7 (35). We found that BFA-induced increase in the expression of CHOP,

260 pri-miR-616, miR-616-5p and miR-616-3p was attenuated in PERK-knockdown sub-clones of
261 MCF7 (**Fig 4A**), whereas knockdown of ATF6 or XBP1 had no significant effect (**Fig 4B-C**).
262 These results suggest that miR-616 is co-transcribed along with the CHOP transcript and
263 attenuated PERK signalling compromised the induction of CHOP mRNA, pri-miR-616, miR-
264 616-5p and miR-616-3p during UPR.
265

266 **Fig 3. Upregulation of miR-616 (5p and 3p) and its host gene CHOP during UPR.** (A) MCF7
267 cells, (B) BT474 cells and (C) HCT116 cells were treated with (1 µM) TG or (0.5 µg/ml) BFA
268 for 24 hours. Expression of CHOP was quantified by RT-qPCR, normalized using RPLP0. The
269 expression level of miR-616 -5p and -3p was quantified by RT-qPCR, normalized using U6
270 snRNA. Error bars represent mean ±S.D. from three independent experiments performed in
271 triplicate. *P < 0.05, two-tailed unpaired t-test as compared to untreated control.
272

273 **Fig 4. Upregulation of miR-616 during ER stress is dependent on PERK pathway.** (A-C)
274 MCF7 PLKO, MCF7 XBP1-KD, MCF7 PERK-KD and MCF7 ATF6-KD sub-clones were treated
275 with (0.5 µg/ml) BFA for 24 hours. Expression level of CHOP and pri-miR-616 was quantified
276 by RT-qPCR, normalizing against RPLP0. The expression level of miR-616 -5p and -3p was
277 quantified by RT-qPCR, normalized using U6 snRNA. *P<0.05, **P < 0.001, two-tailed
278 unpaired t-test. N.S not significant.
279

## 280 MiR-616 targets c-MYC and reduces cell proliferation of breast cancer cells

281 Ye et al. reported that ectopic expression of miR-616-3p inhibited growth of MDA-MB231
282 cells while Arabkari did not find any effect of miR-616 overexpression in MDA-MB231 cells
283 (18) (25). Further, Yuan reported that miR-616-3p promoted growth and migration of MCF7
284 cells in contrast to Arabkari, who reported a decrease in growth and migration of miR-616
285 expressing MCF7 cells (19) (25). This could be due to different approaches used for
286 overexpression of miRNAs. Next, we used gain-of-function (overexpression) and loss-of-
287 function (CRISPR-Cas9 KO) approaches in MCF7 cells to study the role of miR-616 in breast
288 cancer. To better mimic the *in vivo* scenario we decided to use a lentiviral system for
289 modulating the expression of both miR-616-5p and -3p concurrently. For this purpose,

290 MCF7 cells were transduced with lentivirus expressing GFP along with miR-616 or Cas-9
291 along with gRNAs targeting miR-616. The expression of pri-miR-616, miR-616-5p and miR-
292 616-3p was determined in miR-616-overexpressing (MCF7-miR-616-OE) and miR-616-
293 knockout (MCF7-miR-616-KO) sub-clones of MCF7. As expected, the levels of pri-miR-616,
294 miR-616-5p and miR-616-3p were increased in MCF7-miR-616-OE sub-clone (**Fig. 5A**) and
295 decreased in MCF7-miR-616-KO sub-clone (**Fig. 5E**). The MCF7-miR-616-KO sub-clone
296 displayed hypomorphic phenotype with partial reduction in expression of pri-miR-616, miR-
297 616-5p and miR-616-3p. The miR-616 overexpressing (MCF7-miR-616-OE) sub-clone showed
298 significantly decreased cell growth (**Fig. 5B**), while the miR-616 knockout (MCF7-miR-616-
299 KO) sub-clone showed increased cell growth (**Fig. 5F**). This observation was further validated
300 by colony formation assay. The miR-616 overexpressing (MCF7-miR-616-OE) sub-clone of
301 MCF7 cells showed decrease in the number and size of the colonies (**Fig. 5C-D**) but miR-616
302 knockout (MCF7-miR-616-KO) sub-clone showed an increase in the number and size of the
303 colonies (**Fig. 5G-H**). We found that expression of c-MYC mRNA and protein was reduced in
304 miR-616 overexpressing (MCF7-miR-616-OE) sub-clone of MCF7 cells (**Fig. 6 A and C**) and
305 increased in miR-616 knockout (MCF7-miR-616-KO) sub-clone (**Fig. 6 B and C**). Likewise,
306 overexpression of miR-616 in HCT116 cells significantly decreased cell growth and migration
307 that was accompanied by reduced expression of c-MYC (**S1 Fig**). Our results are in
308 agreement with an earlier report where ectopic expression of miR-616 was shown to inhibit
309 growth of MCF7 cells accompanied by reduced expression of c-MYC (25). Since an inverse
310 relationship between the levels of expression of a miRNA and its target is anticipated, we
311 evaluated expression of c-MYC during conditions of UPR. We found the expression of c-MYC
312 mRNA was decreased in MCF7 (**Fig. 7A)** and BT474 (**Fig. 7B**) cells treated either with TG or
313 BFA. Furthermore, expression of c-MYC protein was decreased in MCF7 and BT474 cells

upon treatment with BFA (**Fig. 7C**). These results suggest a role for miR-616 in regulation of c-MYC expression during conditions of UPR.

**Fig 5. MiR-616 reduces the proliferation of MCF7 cells.** (A) The expression of miR-616-3p, miR-616-5p and pri-miR-616 is shown in MCF7-miR-CTRL and MCF7-miR-616-OE sub-clones of MCF7. (B) MCF7-miR-CTRL and MCF7-miR-616-OE cells were plated and cell growth was determined by x-CELLigence. (C-D) MCF7-miR-CTRL and MCF7-miR-616-OE cells were plated in 6- well plate (1000 cells/well) and grown for 14 days. (C) Colonies stained with crystal violet are shown. (D) Quantification of number of colonies for MCF7-miR-CTRL and MCF7-miR-616-OE cells is shown. (E) The expression of miR-616-3p, miR-616-5p and pri-miR-616 is shown in MCF7-Cas9-CTRL and MCF7-miR-616-KO sub-clones of MCF7. (F) MCF7-Cas9-CTRL and MCF7-miR-616-KO cells were plated and cell growth was determined by x-CELLigence. (G-H) MCF7-Cas9-CTRL and MCF7-miR-616-KO cells were plated in 6-well plate (1000 cells/well) and grown for 14 days. (G) Colonies stained with crystal violet are shown. (H) Quantification of number of colonies for MCF7-Cas9-CTRL and MCF7-miR-616-KO cells is shown.

**Fig 6. MiR-616 regulates the expression of c-MYC.** (A-B) Expression level of c-MYC mRNA is shown in miR-616 knockout and miR-616 overexpressing sub-clones of MCF7 cells as determined by qRT-PCR. Error bars represent mean ± S.D. from two independent experiments performed in triplicate. *$P < 0.05$, two-tailed unpaired t-test as compared to control. (C) The expression level of c-MYC protein is shown in miR-616 knockout and miR-616 overexpressing sub-clones of MCF7 cells.

**Fig 7. Downregulation of c-MYC during UPR in breast cancer cells.** (A) MCF7 cells and (B) BT474 cells were treated with (1 µM) TG or (0.5 µg/ml) BFA for 24 hours. Expression of c-MYC was quantified by RT-qPCR, and normalized using RPLP0. Error bars represent mean ±S.D. from three independent experiments performed in triplicate. (C) MCF7 BT474 cells were treated with (0.5 µg/ml) BFA for indicated time points. Western blotting of total protein was performed using antibodies for c-MYC and actin. Representative Immunoblot and quantification of c-MYC expression normalised to actin are shown (n=3). *$P < 0.05$, two-tailed unpaired t-test as compared to the untreated control.

## MiR-616 modulates the expression of c-MYC via site in the ORF

To determine the mechanism of c-MYC regulation by miR-616, we used several bioinformatics tools to search for the potential miR-616 binding sites in the reference sequence of c-MYC. TargetScan (36) did not identify miR-616 binding sites in c-MYC. Interestingly, RNAhybrid identified non-canonical miR-616-5p binding sites (at position 77,

352 2501 and 3076 bp) and miR-616-3p binding sites (at position 614, 917 and 1525 bp) of c-
353 MYC reference Sequence (NM_002467.6) (**S2 Fig**). Furthermore, (miRWALK and RNAhybrid)
354 picked an identical, non-canonical miR-616-3p binding site in the protein-coding region
355 (364-1728 bp) of c-MYC at position 1525 bp (**Fig. 8A-B**). To test whether miR-616 down-
356 regulates c-MYC via this site in coding region, we co-transfected 293T cells with an
357 expression vector containing the ORF of c-MYC and miR-616 plasmid. Cell lysates were
358 collected after 24 h and analysed by immunoblotting. Our results showed that c-MYC
359 protein level was strongly down-regulated by co-expression of miR-616 (**Fig. 8C**). Under
360 similar conditions, co-expression of miR-616 had no effect on protein level of ERα (protein
361 coding region of ERα has no predicted binding sites for miR-616) (**Fig. 8D**). Further, co-
362 expression of miR-4726 (miRNA that lacks binding sites in the protein coding region of c-
363 MYC) and c-MYC had no effect on c-MYC protein level (**Fig. 8E**). Taken together these results
364 suggest that miR-616 regulates the expression of c-MYC most likely via the miR-616
365 response elements present in its protein coding region.

366

367 Fig 8. **Identification of a miR-616-3p-binding sites in the ORF of c-MYC.** Binding site for
368 miR-616-3p identified by (A) miRWALK and (B) RNAhybrid in protein coding region of c-MYC
369 reference sequence is shown. The secondary structure of miRNA-mRNA duplex is shown
370 with miR-616-3p in green and c-MYC mRNA in red. mfe: minimum free energy. (C) 293T cells
371 were transfected with plasmid containing c-MYC ORF in absence and presence of miR-616
372 plasmid. (D) 293T cells were transfected with plasmid containing ERα ORF in absence and
373 presence of miR-616 plasmid. (E) 293T cells were transfected with plasmid containing c-MYC
374 ORF in absence and presence of miR-4726 plasmid. Western blotting of total protein was
375 performed using the indicated antibodies. 24 h post-transfection western blotting of total
376 protein was performed using the indicated antibodies.
377

## 378 Expression of c-MYC can reverse the growth inhibitory effects of miR-616

379 c-Myc is an oncogene frequently overexpressed in human tumours. In light of our results,
380 we reasoned that c-MYC could be the functionally relevant target that mediates tumour-

381 suppressive effects of miR-616. If suppression of c-MYC by miR-616 is indeed crucial for
382 tumour-suppressive effects of miR-616, overexpression of c-MYC should rescue the effect of
383 miR-616 on cell growth. To test this, we transduced lentivirus that express c-MYC into miR-
384 616 expressing MCF7 cells (**Fig. 9A**). We found that expression of c-MYC significantly
385 reversed the growth inhibitory effects of miR-616 in MCF7 cells (**Fig. 9B**). Further, we
386 observed that expression of c-MYC rescued the inhibitory effects of miR-616 on the number
387 and size of the colonies in MCF7 cells (**Fig. 9C**). Next we determined whether c-MYC can
388 rescue the effects of miR-616 on migration of cells. The bright field images of the wound
389 healing revealed that expression of c-MYC restored the rate of wound healing in miR-616
390 expressing MCF7 cells that was comparable to control cells (**Fig. 9D-E**). Thus overexpression
391 of c-MYC rescued the inhibitory effects of miR-616 on cell growth, colony formation and
392 migration. The data therefore suggests an essential role for c-MYC as a mediator of the
393 biological effects of miR-616 in breast cancer cells.
394

395 Figure 9. **Restoration of c-MYC expression overcomes the inhibitory effect of miR-616 on**
396 **cell proliferation.** (A) The expression level of c-MYC protein in MCF7-miR-CTRL and MCF7-
397 miR-616 and MCF7-miR-616 cells transduced with c-MYC lentivirus is shown. (B-C) Cell
398 growth was determined by MTS assay and colony formation assay using MCF7-miR-CTRL
399 and MCF7-miR-616 and MCF7-miR-616 cells expressing c-MYC. (B) Cell proliferation was
400 assessed by MTS assay. Line graphs show the absorbance in cells at the indicated time
401 points. Error bars represent mean ± S.D. from three independent experiments performed in
402 triplicate. (C) Cells were plated in 6-well plate (1000 cells/well) and grown for 14 days.
403 Colonies stained with crystal violet are shown. (D-E) Cells were plated in 6-well plate. The
404 monolayer of cells was scratched with a micropipette tip (200 µl). Black lines indicate the
405 wound borders at indicated time points post-scratching. Scale bar, 1000 µM. Line graph
406 shows the scratch gap quantified using Image J software at the indicated time points. Error
407 bars represent mean ±S.D. from three independent experiments. *P < 0.05.
408

409 **Prognostic value of the miR-616 in human cancers**

410 We assessed the prognostic value of miR-616 in different cancer types using KM plotter. We
411 found that expression of miR-616 was associated with longer overall survival (OS) in cervical
412 squamous cell carcinoma, Head-neck squamous cell carcinoma, uterine corpus endometrial
413 carcinoma and Thymoma (**S3 Fig**). Surprisingly, the increased expression of miR-616 was
414 associated with shorter OS in esophageal adenocarcinoma, sarcoma, renal clear cell
415 carcinoma, lung squamous cell carcinoma and hepatocellular carcinoma (**S3 Fig**). Next, we
416 used TNMplot to determine the expression of CHOP and miR-616 in normal and tumour
417 tissue samples of breast. We found that expression of CHOP and miR-616 was reduced in
418 tumour samples as compared to tumour adjacent normal tissue (**Fig. 10A-B**). Further, the
419 expression of miR-616 was associated with poor OS in luminal A subtype and better OS
420 HER2 subtype of breast cancer (**Fig. 10C**).

421 **Fig 10. Prognostic value of miR-616 in subtypes of breast cancer.** TNMplot
422 (https://tnmplot.com/analysis/) was used to determine the expression of CHOP and miR-
423 616 in human breast cancer. (A) Box plot for expression of CHOP in tumour (n=1097) and
424 normal (n=403) tissues for human breast cancers is shown. (B) Box plot for expression of
425 miR-616 in paired tumour (n=112) and tumour adjacent normal (n=112) for human breast
426 cancers is shown. (C) KM Plotter (https://kmplot.com/) was used to determine the
427 association of miR-616 with overall survival (OS) in subtypes of breast cancer.
428

429 # DISCUSSION

430 MiRNAs regulate the wide range of cellular processes because of their ability to alter post-
431 transcriptional gene expression (37). We have evaluated the role of UPR regulated miRNA-
432 616 in cell growth and proliferation. We have shown that expression of miR-616 and its host
433 gene (CHOP) is upregulated during ER stress in a PERK-dependent fashion (**Fig 4**). ER stress
434 and UPR activation contributes to the initiation and progression of human diseases, such as
435 cancer, neurodegenerative and cardiovascular disease (2, 38). We observed concordant
436 expression of the CHOP and the mature miR-616 which suggests their transcriptional co-

437 regulation (**Fig 3, 4**). Our results suggest a mechanism for increased expression of miR-616
438 in patho-physiological conditions where role of UPR is implicated.
439
440 Several studies have reported that miR-616 acts as a tumour promoting miRNA in human
441 cancers (11, 31, 39). However, our results show that miR-616 expression attenuates the
442 proliferation of MCF7 cells while reduced expression of miR-616 increases it (**Fig 5**).
443 Furthermore, we observed that expression of miR-616 was reduced in human breast
444 cancers as compared to tumour adjacent normal tissue (**Fig 10**). In agreement with our
445 results miR-616-3p has been shown to potentiate apoptosis in HUVECs (16), inhibit head
446 and neck squamous cell carcinoma progression (17) and inhibit cell growth and
447 mammosphere formation of breast cancer cells (18, 25). Any small RNA having G-rich 6mer
448 seed sequence (nt 2-7 of the guide strand) can reduce viability of cells when associated with
449 RNA-induced silencing complex. G-rich seed sequence mediates toxicity by targeting C-rich
450 seed matches in the 3′ UTR of genes critical for cell survival referred to as Death Induced by
451 Survival gene Elimination (DISE) (30). A systematic study to evaluate DISE activity of all 4096
452 possible 6mer seed sequences in six cell lines (three human and three mouse) revealed the
453 mechanism underlying this toxicity and a web-based algorithm (https://6merdb.org) can
454 predict the activity of an RNA with a known 6mer seed (40). Analysis of seed sequences
455 from both 5p and 3p strands of miR-616 revealed that both strands can exhibit opposing
456 effects on viability in a cell-type dependent manner (**S4 Fig**). Interestingly, several miRNAs
457 belonging to miR-371-373 Cluster (hsa-miR-371a-5p, hsa-miR-371b-5p, hsa-miR-372-5p and
458 hsa-miR-373-5p) that share seed sequence with miR-616-5p, have been shown to reduce
459 the progression and metastasis of colon cancer (41) as well as induction of cell cycle arrest
460 (42). Taken together, these observations indicate the presence of context-dependent

461 oncogenic and tumour suppressive effects of miR-616 in human cancers. Indeed context-
462 dependent tumour-promoting and tumour-suppressive role has been documented for
463 several miRNAs such as miR-17-92 cluster (43, 44). This cluster maps to a region frequently
464 amplified in Burkitt's lymphoma, diffuse large B-cell lymphoma, follicular lymphoma and
465 lung cancer (26, 43). The expression of miR-17-92 is reduced in prostate cancer (17) and
466 miR-17-92 expression in intestinal epithelial cells inhibited colon cancer progression by
467 suppressing tumour angiogenesis (17).
468
469 Studies on target recognition by miRNAs have shown that sequence complementarity at the
470 5' end of the miRNA, the so-called "seed region" at positions 2 to 7, is a main determinant
471 for target recognition (36). However, a perfect seed match of its own is not a good predictor
472 for miRNA regulation and a number of studies have shown that miRNA can regulate the
473 expression of target genes via the sites with a G: U wobble and/or mismatch in the seed
474 region (36). Further, a study using a cross-linking and immunoprecipitation method to
475 experimentally identify microRNA target sites in an unbiased manner has reported a
476 significant number of non-canonical sites (45, 46). Hence, presence of perfect seed
477 complementarity is not essential for regulation of target genes by miRNA. In addition, target
478 sites for endogenous miRNAs have been reported in ORFs and 5′ UTRs, but they are less
479 frequent than those in the 3' UTR (47, 48). We found a non-canonical miR-616-3p binding
480 site in the protein coding region of c-MYC transcript (**Fig 8**). Several studies have reported
481 the presence of miRNA-binding sites in the protein coding sequence of the genes. Indeed
482 miRNAs have been shown to regulate embryonic stem cell differentiation, DNA methylation,
483 regulation of apoptosis, aortic development, and tumour suppression via the functional
484 miRNA-binding sites in the protein coding sequence of the target genes (47, 48, 49). Several

485 studies have reported the upregulation of c-MYC in different cancer cells and tumours such
486 as neuroblastomas, lung, and breast cancer (50). The expression of c-MYC was
487 downregulated in miR-616 expressing and upregulated in miR-616 knockout MCF7 cells (**Fig**
488 **6**). These observations suggest that effects of miR-616 on cell growth are primarily mediated
489 by downregulation of c-MYC.
490
491 PERK has been shown to act as a haploinsufficient tumour suppressor, where the nature of
492 its function is determined by gene dose (51, 52). Transient pause in protein synthesis due to
493 eIF2α phosphorylation by PERK is beneficial by reducing secretory load in the ER.
494 Phosphorylation of NRF2 by PERK attenuates Keap1-mediated degradation of NRF2 and
495 promotes expression of anti-oxidant enzymes through the antioxidant response elements
496 (53, 54). PERK signalling can upregulate the CHOP/DDIT3 transcription factor, which inhibits
497 expression of the gene encoding anti-apoptotic BCL-2 to hasten cell death, in addition to
498 enhancing the expression of pro-apoptotic BCL-2 members such as BIM (54). Studies in both
499 cellular and animal models with CHOP gene deficiency have shed light on the pro-apoptotic
500 role of CHOP during cellular stress (54). Further, ectopic expression of CHOP was reported to
501 induce a G1 cell cycle arrest (55). CHOP maintains the integrity of the human hematopoietic
502 stem cell (HSC) pool by eliminating HSCs harbouring oncogenic mutations, and decrease the
503 risk of leukaemia. CHOP induction triggers apoptosis of premalignant cells to prevent
504 malignant progression in a mouse lung cancer model. Hepatocyte-specific CHOP ablation
505 increased tumourigenesis in high fat diet-induced steatohepatitis and Hepatocellular
506 carcinoma (56, 57). CHOP has been shown to promote cancer progression, when fused with
507 FUS/TLS or EWS protein by genomic rearrangement (58, 59). The FUS-CHOP oncoprotein has
508 been shown to induce metastasis in in vivo model of sarcoma (58). Accumulating data

509 suggest that CHOP impinges upon several aspects of cancer including initiation as well as
510 progression of tumours (54). Our results show that miR-616 supressed cell growth of cancer
511 cells through suppressing c-MYC expression. Our results establish a new and unexpected
512 role for the CHOP locus by providing evidence that miR-616 can inhibit cell proliferation by
513 targeting c-MYC.
514

515 # ACKNOWLEDGEMENTS

516 We are grateful to the Technical Officers and administrative team in Pathology, School of
517 Medicine at University of Galway, Ireland.
518

519 # REFERENCES

520 1. Hetz C, Zhang K, Kaufman RJ. Mechanisms, regulation and functions of the unfolded protein
521 response. Nat Rev Mol Cell Biol. 2020;21(8):421-38.
522 2. Hetz C, Axten JM, Patterson JB. Pharmacological targeting of the unfolded protein response
523 for disease intervention. Nat Chem Biol. 2019;15(8):764-75.
524 3. Barua D, Gupta A, Gupta S. Targeting the IRE1-XBP1 axis to overcome endocrine resistance
525 in breast cancer: Opportunities and challenges. Cancer Lett. 2020;486:29-37.
526 4. Nadanaka S, Okada T, Yoshida H, Mori K. Role of disulfide bridges formed in the luminal
527 domain of ATF6 in sensing endoplasmic reticulum stress. Mol Cell Biol. 2007;27(3):1027-43.
528 5. Yoshida H, Okada T, Haze K, Yanagi H, Yura T, Negishi M, et al. ATF6 activated by proteolysis
529 binds in the presence of NF-Y (CBF) directly to the cis-acting element responsible for the mammalian
530 unfolded protein response. Mol Cell Biol. 2000;20(18):6755-67.
531 6. Cullinan SB, Zhang D, Hannink M, Arvisais E, Kaufman RJ, Diehl JA. Nrf2 is a direct PERK
532 substrate and effector of PERK-dependent cell survival. Mol Cell Biol. 2003;23(20):7198-209.
533 7. Harding HP, Zhang Y, Bertolotti A, Zeng H, Ron D. Perk is essential for translational regulation
534 and cell survival during the unfolded protein response. Mol Cell. 2000;5(5):897-904.
535 8. Ha M, Kim VN. Regulation of microRNA biogenesis. Nat Rev Mol Cell Biol. 2014;15(8):509-24.
536 9. Ma S, Chan YP, Kwan PS, Lee TK, Yan M, Tang KH, et al. MicroRNA-616 induces androgen-
537 independent growth of prostate cancer cells by suppressing expression of tissue factor pathway
538 inhibitor TFPI-2. Cancer Res. 2011;71(2):583-92.
539 10. Zhang S, Zhang X, Chen G, Zheng X, Zhu X, Shan L. Hsa_circ_0007494 suppresses prostate
540 cancer progression via miR-616/PTEN axis. Exp Cell Res. 2020;395(2):112233.
541 11. Wu ZH, Lin C, Liu CC, Jiang WW, Huang MZ, Liu X, et al. MiR-616-3p promotes angiogenesis
542 and EMT in gastric cancer via the PTEN/AKT/mTOR pathway. Biochem Biophys Res Commun.
543 2018;501(4):1068-73.

544 12. Wang DX, Zou YJ, Zhuang XB, Chen SX, Lin Y, Li WL, et al. Sulforaphane suppresses EMT and
545 metastasis in human lung cancer through miR-616-5p-mediated GSK3β/β-catenin signaling
546 pathways. Acta Pharmacol Sin. 2017;38(2):241-51.
547 13. Zhang D, Zhou P, Wang W, Wang X, Li J, Sun X, et al. MicroRNA-616 promotes the migration,
548 invasion and epithelial-mesenchymal transition of HCC by targeting PTEN. Oncol Rep.
549 2016;35(1):366-74.
550 14. Bai QL, Hu CW, Wang XR, Shang JX, Yin GF. MiR-616 promotes proliferation and inhibits
551 apoptosis in glioma cells by suppressing expression of SOX7 via the Wnt signaling pathway. Eur Rev
552 Med Pharmacol Sci. 2017;21(24):5630-7.
553 15. Fan MQ, Huang CB, Gu Y, Xiao Y, Sheng JX, Zhong L. Decrease expression of microRNA-20a
554 promotes cancer cell proliferation and predicts poor survival of hepatocellular carcinoma. J Exp Clin
555 Cancer Res. 2013;32(1):21.
556 16. Chen H, Liu X, Wu Y, Wu X, Wen X, Lu Y, et al. Apoptosis in HUVECs induced by microRNA-
557 616-3p via X-linked inhibitor of apoptosis protein targeting. Exp Ther Med. 2021;21(6):661.
558 17. Hou Y, Zhou M, Li Y, Tian T, Sun X, Chen M, et al. Risk SNP-mediated LINC01614 upregulation
559 drives head and neck squamous cell carcinoma progression via PI3K/AKT signaling pathway. Mol
560 Carcinog. 2022;61(8):797-811.
561 18. Ye G, Pan R, Zhu L, Zhou D. Circ_DCAF6 potentiates cell stemness and growth in breast
562 cancer through GLI1-Hedgehog pathway. Exp Mol Pathol. 2020;116:104492.
563 19. Yuan C. miR-616 promotes breast cancer migration and invasion by targeting TIMP2 and
564 regulating MMP signaling. Oncol Lett. 2019;18(3):2348-55.
565 20. Gupta A, Hossain MM, Read DE, Hetz C, Samali A, Gupta S. PERK regulated miR-424(322)-503
566 cluster fine-tunes activation of IRE1 and ATF6 during Unfolded Protein Response. Sci Rep.
567 2015;5:18304.
568 21. Gupta S, Read DE, Deepti A, Cawley K, Gupta A, Oommen D, et al. Perk-dependent
569 repression of miR-106b-25 cluster is required for ER stress-induced apoptosis. Cell Death Dis.
570 2012;3(6):e333.
571 22. Cawley K, Logue SE, Gorman AM, Zeng Q, Patterson J, Gupta S, et al. Disruption of microRNA
572 biogenesis confers resistance to ER stress-induced cell death upstream of the mitochondrion. PLoS
573 One. 2013;8(8):e73870.
574 23. Read DE, Gupta A, Ladilov Y, Samali A, Gupta S. miRNA signature of unfolded protein
575 response in H9c2 rat cardiomyoblasts. Cell Biosci. 2014;4(1):56.
576 24. Hiramatsu N, Chiang K, Aivati C, Rodvold JJ, Lee JM, Han J, et al. PERK-mediated induction of
577 microRNA-483 disrupts cellular ATP homeostasis during the unfolded protein response. J Biol Chem.
578 2020;295(1):237-49.
579 25. Arabkari V. *Regulation of cell fate by microRNAs during unfolded protein response*
580 *and its role in cancer* [Doctor of Philosophy]. Galway: National University of Ireland Galway, Ireland;
581 (2018) https://aran.library.nuigalway.ie/handle/10379/14750.
582 26. Hossain MM, Sultana A, Barua D, Islam MN, Gupta A, Gupta S. Differential expression,
583 function and prognostic value of miR-17-92 cluster in ER-positive and triple-negative breast cancer.
584 Cancer Treat Res Commun. 2020;25:100224.
585 27. Salim U, Kumar A, Kulshreshtha R, Vivekanandan P. Biogenesis, characterization, and
586 functions of mirtrons. Wiley Interdiscip Rev RNA. 2022;13(1):e1680.
587 28. Mitra R, Lin CC, Eischen CM, Bandyopadhyay S, Zhao Z. Concordant dysregulation of miR-5p
588 and miR-3p arms of the same precursor microRNA may be a mechanism in inducing cell proliferation
589 and tumorigenesis: a lung cancer study. RNA. 2015;21(6):1055-65.
590 29. Kozomara A, Griffiths-Jones S. miRBase: annotating high confidence microRNAs using deep
591 sequencing data. Nucleic Acids Res. 2014;42(Database issue):D68-73.
592 30. Putzbach W, Gao QQ, Patel M, Haluck-Kangas A, Murmann AE, Peter ME. DISE: A Seed-
593 Dependent RNAi Off-Target Effect That Kills Cancer Cells. Trends Cancer. 2018;4(1):10-9.

31. Ren W, Hu J, Li H, Chen J, Ding J, Zu X, et al. miR-616-5p Promotes Invasion and Migration of Bladder Cancer. Front Oncol. 2021;11:762946.
32. Baskerville S, Bartel DP. Microarray profiling of microRNAs reveals frequent coexpression with neighboring miRNAs and host genes. RNA. 2005;11(3):241-7.
33. Schanen BC, Li X. Transcriptional regulation of mammalian miRNA genes. Genomics. 2011;97(1):1-6.
34. Agranat-Tamir L, Shomron N, Sperling J, Sperling R. Interplay between pre-mRNA splicing and microRNA biogenesis within the supraspliceosome. Nucleic Acids Res. 2014;42(7):4640-51.
35. Hossain MM, Barua D, Arabkari V, Islam N, Gupta A, Gupta S. Hyperactivation of nuclear receptor coactivators induces PERK-dependent cell death. Oncotarget. 2018;9(14):11707-21.
36. Agarwal V, Bell GW, Nam JW, Bartel DP. Predicting effective microRNA target sites in mammalian mRNAs. Elife. 2015;4.
37. Jin HY, Xiao C. MicroRNA Mechanisms of Action: What have We Learned from Mice? Front Genet. 2015;6:328.
38. Doyle KM, Kennedy D, Gorman AM, Gupta S, Healy SJ, Samali A. Unfolded proteins and endoplasmic reticulum stress in neurodegenerative disorders. J Cell Mol Med. 2011;15(10):2025-39.
39. Zhou Y, Meng P, Tang B, Ke Z, Liu L, Chen Y, et al. MiR-616 promotes the progression of pancreatic carcinoma by targeting OXR1. Minerva Med. 2021;112(4):528-9.
40. Bartom ET, Kocherginsky M, Paudel B, Vaidyanathan A, Haluck-Kangas A, Patel M, et al. SPOROS: A pipeline to analyze DISE/6mer seed toxicity. PLoS Comput Biol. 2022;18(3):e1010022.
41. Ullmann P, Rodriguez F, Schmitz M, Meurer SK, Qureshi-Baig K, Felten P, et al. The miR-371~373 Cluster Represses Colon Cancer Initiation and Metastatic Colonization by Inhibiting the TGFBR2/ID1 Signaling Axis. Cancer Res. 2018;78(14):3793-808.
42. Langroudi L, Jamshidi-Adegani F, Shafiee A, Rad SM, Keramati F, Azadmanesh K, et al. MiR-371-373 cluster acts as a tumor-suppressor-miR and promotes cell cycle arrest in unrestricted somatic stem cells. Tumour Biol. 2015;36(10):7765-74.
43. Zhao W, Gupta A, Krawczyk J, Gupta S. The miR-17-92 cluster: Yin and Yang in human cancers. Cancer Treat Res Commun. 2022;33:100647.
44. Yu L, Ma W, Song B, Wang S, Li X, Wang Z. Hsa_circ_0030042 Ameliorates Oxidized Low-Density Lipoprotein-Induced Endothelial Cell Injury via the MiR-616-3p/RFX7 Axis. Int Heart J. 2022;63(4):763-72.
45. Stavast CJ, Erkeland SJ. The Non-Canonical Aspects of MicroRNAs: Many Roads to Gene Regulation. Cells. 2019;8(11).
46. Dai W, Su X, Zhang B, Wu K, Zhao P, Yan Z. An Alternative Class of Targets for microRNAs Containing CG Dinucleotide. Biology (Basel). 2022;11(3).
47. Qin W, Shi Y, Zhao B, Yao C, Jin L, Ma J, et al. miR-24 regulates apoptosis by targeting the open reading frame (ORF) region of FAF1 in cancer cells. PLoS One. 2010;5(2):e9429.
48. Duursma AM, Kedde M, Schrier M, le Sage C, Agami R. miR-148 targets human DNMT3b protein coding region. RNA. 2008;14(5):872-7.
49. Tay Y, Zhang J, Thomson AM, Lim B, Rigoutsos I. MicroRNAs to Nanog, Oct4 and Sox2 coding regions modulate embryonic stem cell differentiation. Nature. 2008;455(7216):1124-8.
50. Dang CV. MYC on the path to cancer. Cell. 2012;149(1):22-35.
51. Pytel D, Gao Y, Mackiewicz K, Katlinskaya YV, Staschke KA, Paredes MC, et al. PERK Is a Haploinsufficient Tumor Suppressor: Gene Dose Determines Tumor-Suppressive Versus Tumor Promoting Properties of PERK in Melanoma. PLoS Genet. 2016;12(12):e1006518.
52. Gupta S, Giricz Z, Natoni A, Donnelly N, Deegan S, Szegezdi E, et al. NOXA contributes to the sensitivity of PERK-deficient cells to ER stress. FEBS Lett. 2012;586(22):4023-30.
53. Pytel D, Majsterek I, Diehl JA. Tumor progression and the different faces of the PERK kinase. Oncogene. 2016;35(10):1207-15.
54. Oyadomari S, Mori M. Roles of CHOP/GADD153 in endoplasmic reticulum stress. Cell Death Differ. 2004;11(4):381-9.

645 55. Jauhiainen A, Thomsen C, Strombom L, Grundevik P, Andersson C, Danielsson A, et al.
646 Distinct cytoplasmic and nuclear functions of the stress induced protein DDIT3/CHOP/GADD153.
647 PLoS One. 2012;7(4):e33208.
648 56. Toriguchi K, Hatano E, Tanabe K, Takemoto K, Nakamura K, Koyama Y, et al. Attenuation of
649 steatohepatitis, fibrosis, and carcinogenesis in mice fed a methionine-choline deficient diet by
650 CCAAT/enhancer-binding protein homologous protein deficiency. J Gastroenterol Hepatol.
651 2014;29(5):1109-18.
652 57. Rahman SM, Schroeder-Gloeckler JM, Janssen RC, Jiang H, Qadri I, Maclean KN, et al.
653 CCAAT/enhancing binding protein beta deletion in mice attenuates inflammation, endoplasmic
654 reticulum stress, and lipid accumulation in diet-induced nonalcoholic steatohepatitis. Hepatology.
655 2007;45(5):1108-17.
656 58. Pérez-Losada J, Pintado B, Gutiérrez-Adán A, Flores T, Bañares-González B, del Campo JC, et
657 al. The chimeric FUS/TLS-CHOP fusion protein specifically induces liposarcomas in transgenic mice.
658 Oncogene. 2000;19(20):2413-22.
659 59. Matsui Y, Ueda T, Kubo T, Hasegawa T, Tomita Y, Okamoto M, et al. A novel type of EWS-
660 CHOP fusion gene in myxoid liposarcoma. Biochem Biophys Res Commun. 2006;348(2):437-40.

661

662 # Supporting information

663 S1 Fig. **miR-616 reduces the proliferation of HCT116 cells.** (A) Control (HCT116-miR-CTRL)
664 and miR-616-overexpressing (HCT116-miR-616) sub-clones of HCT116 cells were plated and
665 cell growth was determined by MTS assay. Line graphs show the absorbance in cells at the
666 indicated time points. Error bars represent mean ± S.D. from three independent
667 experiments performed in triplicate. (B) HCT116-miR-CTRL and HCT116-miR-616 cells were
668 plated in 6- well plate (1000 cells/well) and grown for 14 days. Colonies stained with crystal
669 violet are shown. (C) HCT116-miR-CTRL and HCT116-miR-616 cells were plated in 6-well
670 plate. The monolayer of cells was scratched with a micropipette tip (200 µl). Black lines
671 indicate the wound borders at indicated time points post-scratching. Scale bar, 1000 µM.
672 Line graph shows the scratch gap quantified using Image J software at the indicated time
673 points. (D) The expression level of c-Myc protein is shown in HCT116-miR-CTRL and HCT116-
674 miR-616 cells. *P < 0.05, two-tailed unpaired t-test as compared to the control sub-clone.

675

676 S2Fig. **Identification of a miR-616-5p and miR-616-3p -binding sites in the c-Myc.**
677 RNAhybrid analysis of c-MYC reference sequence and miR-616. The secondary structure of
678 miRNA-mRNA duplex is shown with miRNA in green and mRNA in red. mfe: minimum free
679 energy.

680

681 S3 Fig. **Association between miR-616 expression and overall survival in human cancer**.
682 Web-based algorithm KM plotter (http://kmplot.com/analysis/) was used to evaluate the
683 association between miR-616 with overall (OS) survival.

684

685 S4 Fig. **Prediction of the effect of miR-616-5p and miR-616-3p on cell viability through their**
686 **6mer seed sequence.** The activity of 6-mer seed of was evaluated in three human (HeyA8-
687 ovarian, H460-lung and H4-brain) and three mouse (M565-liver, 3LL-lung and GL261-brain)
688 cell lines. MiRNAs with low viability (high toxicity) are shown in red and with high viability
689 (low toxicity) are shown in green. Predominantly expressed mature miRNAs (guide miRNA)
690 are shown in dark purple while lesser expressed (passenger miRNA) are shown in light
691 purple. The miRNAs sharing seed sequence with miR-616-5p are also shown.

A

B

CHOP (NM_001195053.1)

| miRNA | Other name | Accession number | Sequence 5' to 3' |
|---|---|---|---|
| hsa-miR-616-5p | hsa-miR-616* | MIMAT0003284 | ACUCAAAACCCUUCAGUGACUU |
| hsa-miR-616-3p | hsa-miR-616 | MIMAT0004805 | AGUCAUUGGAGGGUUUGAGCAG |

C

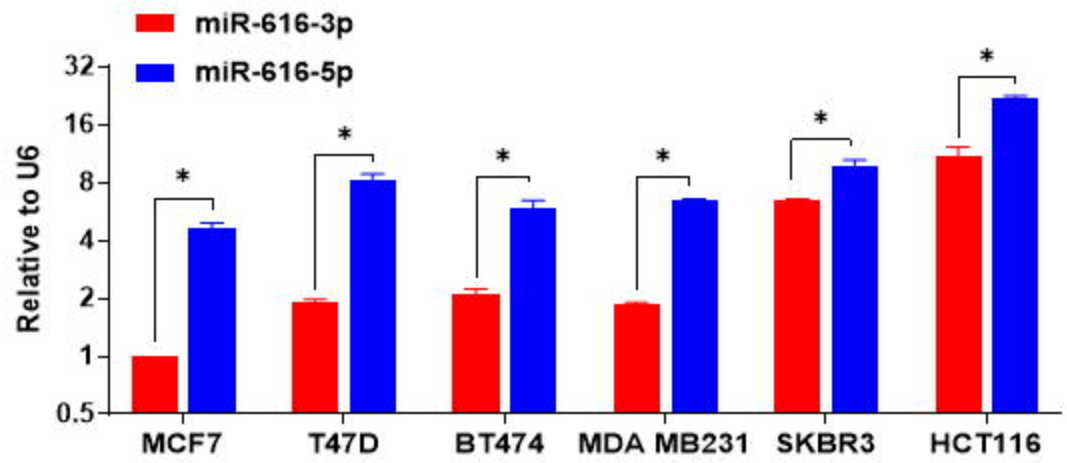


Figure 1

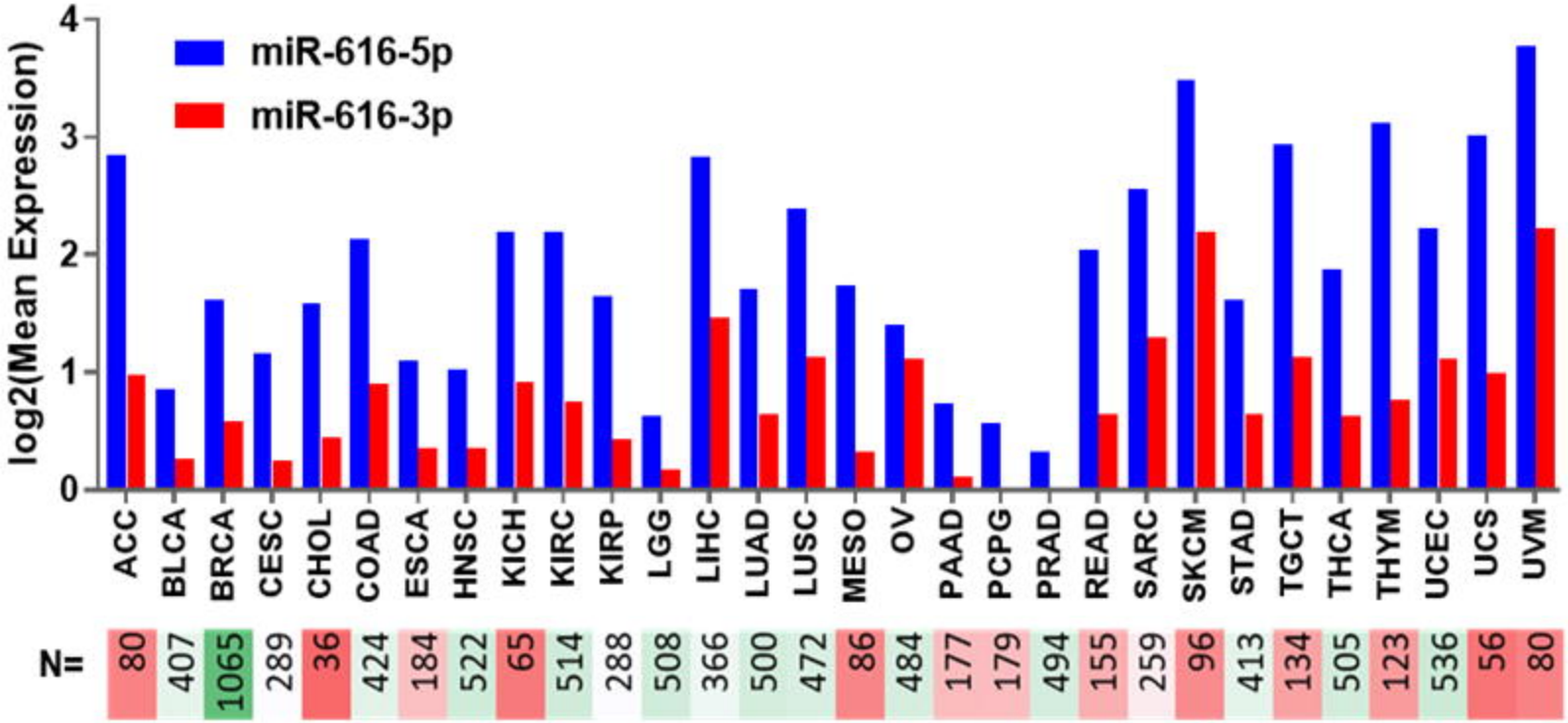
log2(Mean Expression)
miR-616-5p
miR-616-3p
0
1
2
3
4
ACC
BLCA
BRCA
CESC
CHOL
COAD
ESCA
HNSC
KICH
KIRC
KIRP
LGG
LIHC
LUAD
LUSC
MESO
OV
PAAD
PCPG
PRAD
READ
SARC
SKCM
STAD
TGCT
THCA
THYM
UCEC
UCS
UVM
N=
80
407
1065
289
36
424
184
522
65
514
288
508
366
500
472
86
484
177
179
494
155
259
96
413
134
505
123
536
56
80

Figure 2

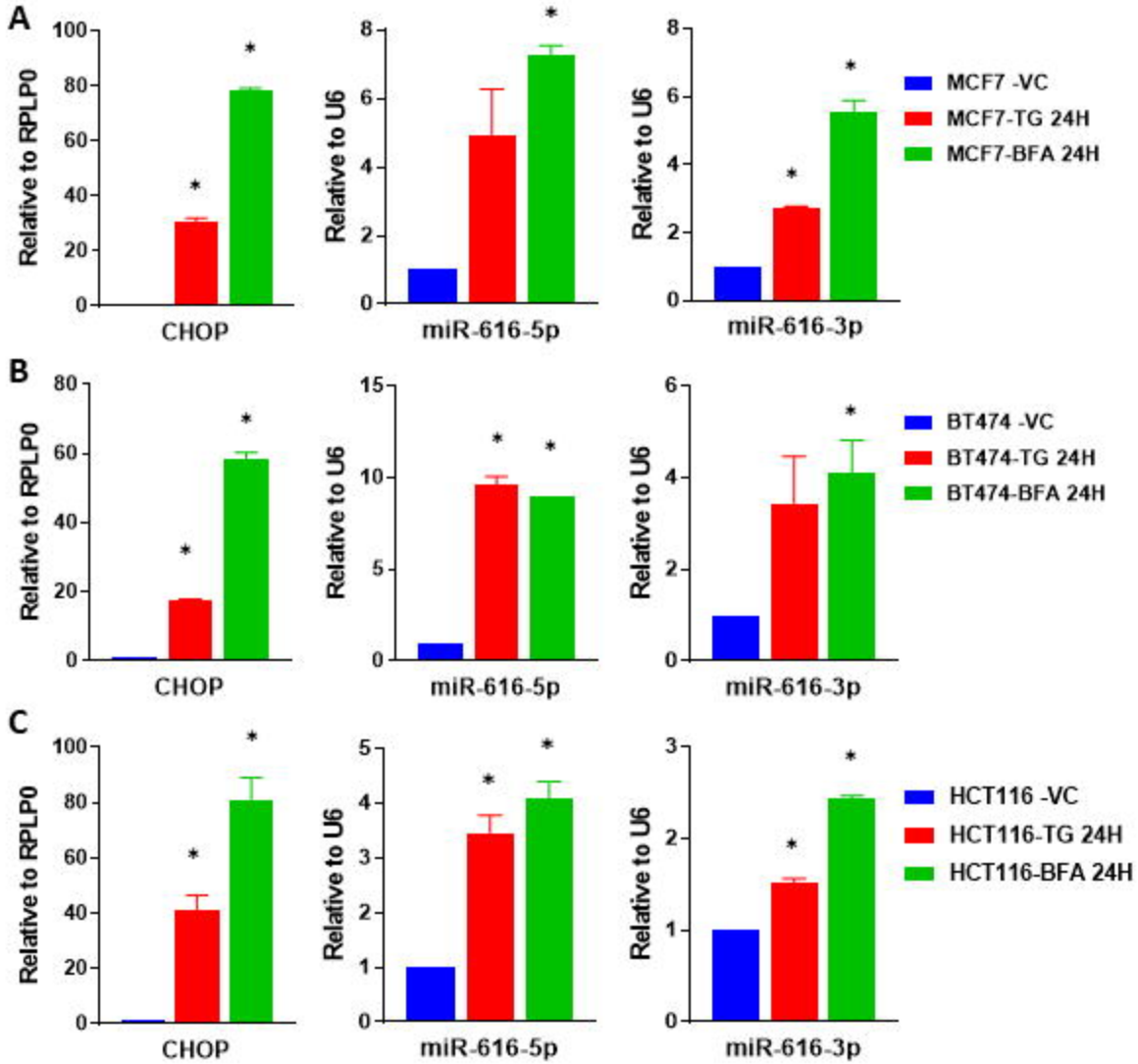
A
Relative to RPLP0
CHOP
Relative to U6
miR-616-5p
miR-616-3p
MCF7 -VC
MCF7-TG 24H
MCF7-BFA 24H
B
BT474 -VC
BT474-TG 24H
BT474-BFA 24H
C
HCT116 -VC
HCT116-TG 24H
HCT116-BFA 24H

**Figure 3**

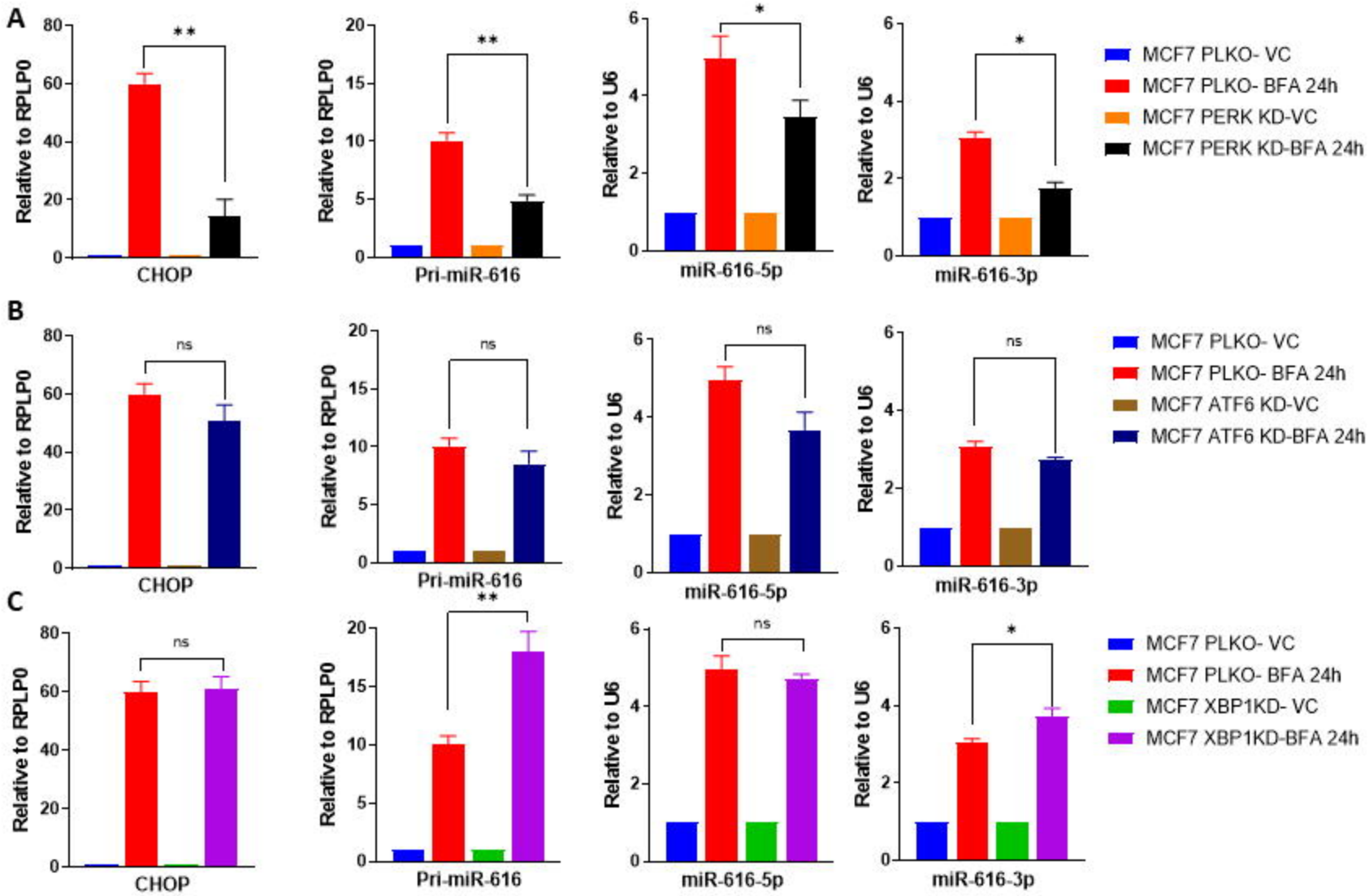
A
B
C
Relative to RPLP0
Relative to U6
CHOP
Pri-miR-616
miR-616-5p
miR-616-3p
**
*
ns
MCF7 PLKO- VC
MCF7 PLKO- BFA 24h
MCF7 PERK KD-VC
MCF7 PERK KD-BFA 24h
MCF7 ATF6 KD-VC
MCF7 ATF6 KD-BFA 24h
MCF7 XBP1KD- VC
MCF7 XBP1KD-BFA 24h

**Figure 4**

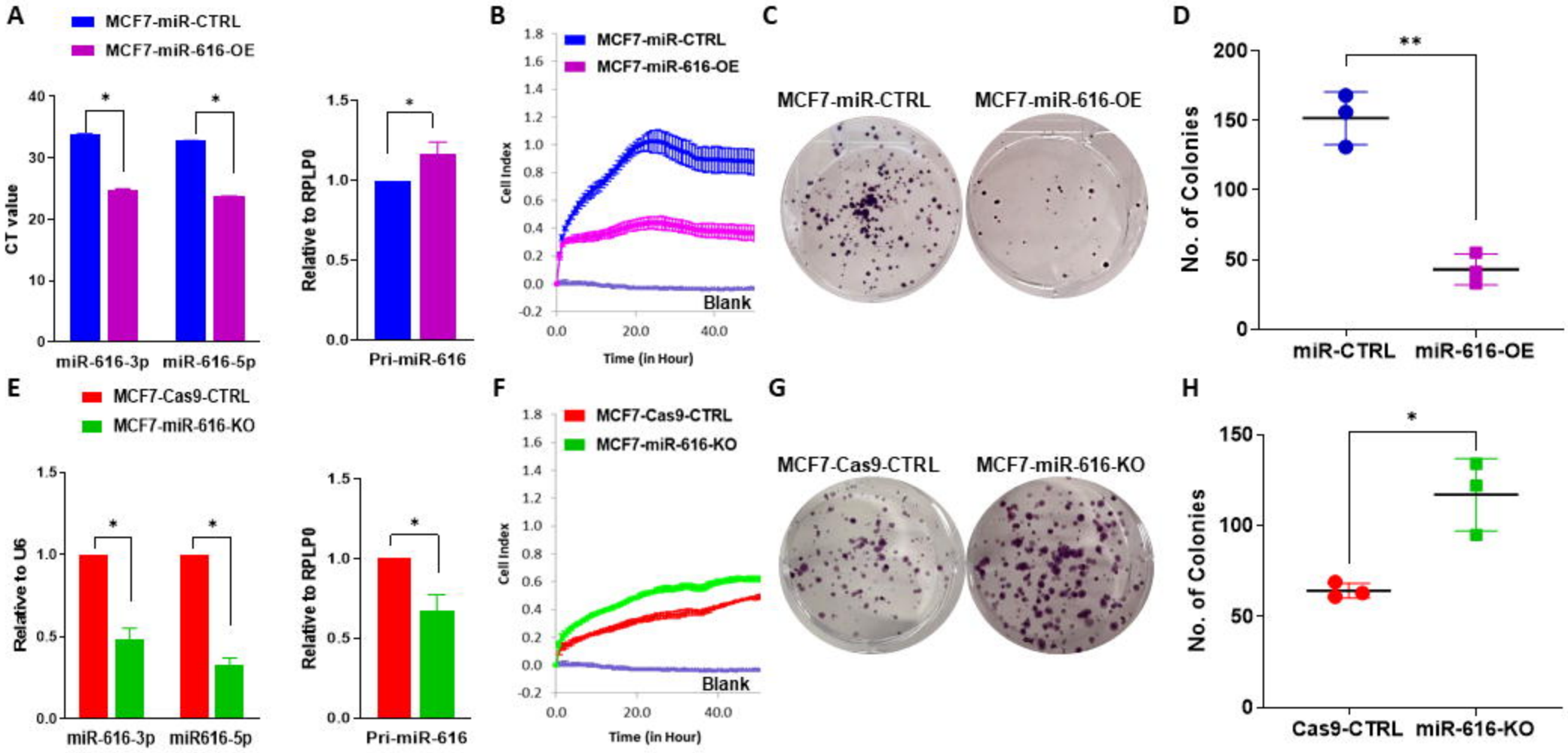
A
MCF7-miR-CTRL
MCF7-miR-616-OE
CT value
miR-616-3p
miR-616-5p
Relative to RPLP0
Pri-miR-616
B
MCF7-miR-CTRL
MCF7-miR-616-OE
Cell Index
Blank
Time (in Hour)
C
MCF7-miR-CTRL
MCF7-miR-616-OE
D
No. of Colonies
miR-CTRL
miR-616-OE
E
MCF7-Cas9-CTRL
MCF7-miR-616-KO
Relative to U6
miR-616-3p
miR616-5p
Relative to RPLP0
Pri-miR-616
F
MCF7-Cas9-CTRL
MCF7-miR-616-KO
Cell Index
Blank
Time (in Hour)
G
MCF7-Cas9-CTRL
MCF7-miR-616-KO
H
No. of Colonies
Cas9-CTRL
miR-616-KO

**Figure 5**

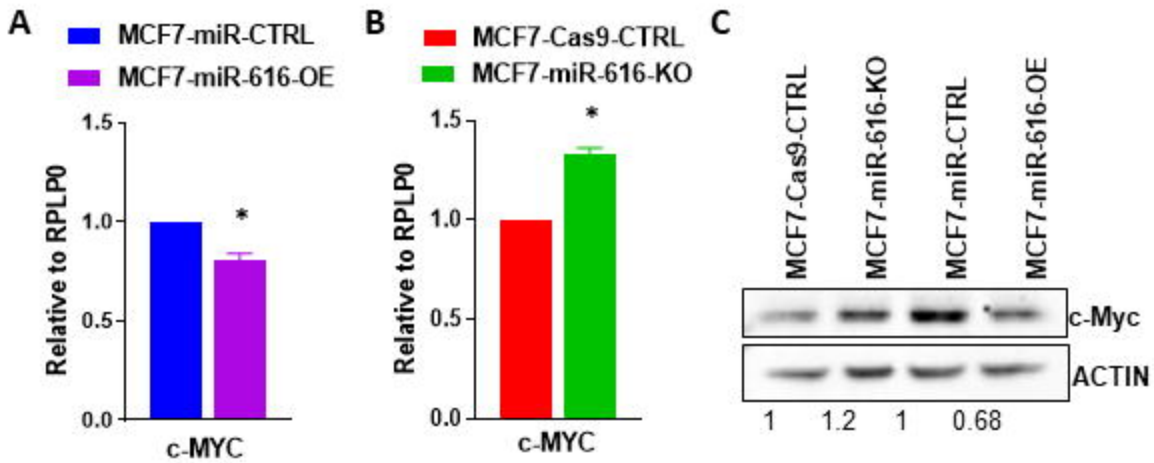
A
MCF7-miR-CTRL
MCF7-miR-616-OE
Relative to RPLP0
1.5
1.0
0.5
0.0
*
c-MYC
B
MCF7-Cas9-CTRL
MCF7-miR-616-KO
Relative to RPLP0
1.5
1.0
0.5
0.0
*
c-MYC
C
MCF7-Cas9-CTRL
MCF7-miR-616-KO
MCF7-miR-CTRL
MCF7-miR-616-OE
c-Myc
ACTIN
1
1.2
1
0.68

**Figure 6**

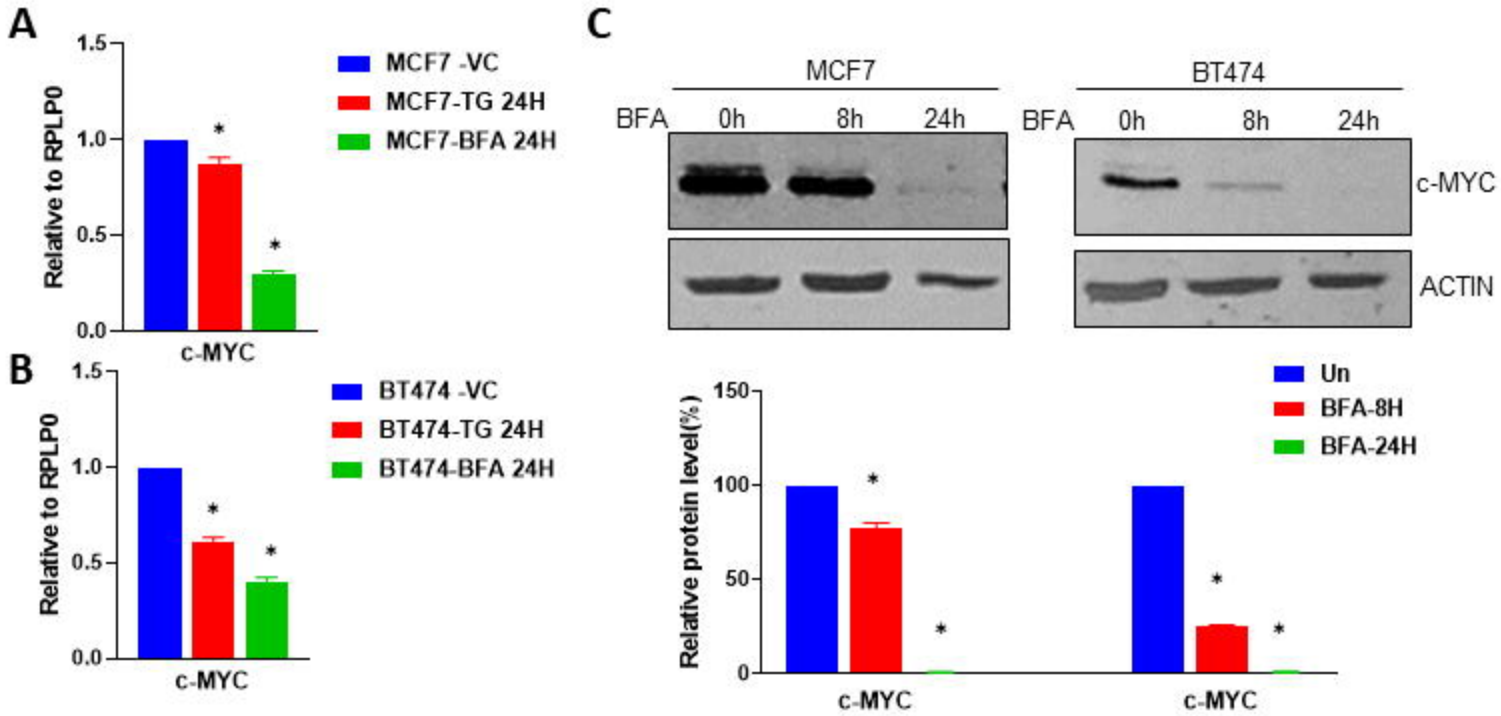
A
1.5
1.0
0.5
0.0
Relative to RPLP0
c-MYC
MCF7 -VC
MCF7-TG 24H
MCF7-BFA 24H
B
1.5
1.0
0.5
0.0
Relative to RPLP0
c-MYC
BT474 -VC
BT474-TG 24H
BT474-BFA 24H
C
MCF7
BT474
BFA
0h
8h
24h
BFA
0h
8h
24h
c-MYC
ACTIN
150
100
50
0
Relative protein level(%)
c-MYC
c-MYC
Un
BFA-8H
BFA-24H

**Figure 7**

**A**

| | |
|---|---|
| miRNA | hsa-miR-616-3p |
| RefseqID | NM_002467 |
| GeneSymbol | MYC |
| Binding Site | 1525.1546 |
| Score | 0.846 |
| Seed | 0 |
| Au | 0.515 |
| Energy | -20.3 |
| Binding Len | 21 |
| Me | -7.719 |
| Phylopstem | 0.0 |
| Phylopflank | 0.0 |
| Longest Consecutive Pairings | 6 |
| Position Of Longest Consecutive Pairings | 1 |
| Pairings In 3prime End | 4 |
| Position | CDS |

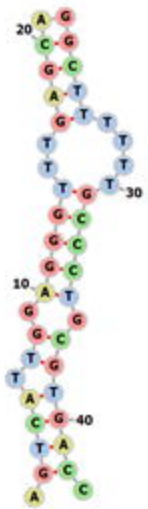


**B**

```
Target: NM_002467.6
length: 3721
MiRNA: hsa-miR-616-3p
length: 22

mfe: -25.0 kcal/mol
p-value: 1.000000e+00

Position: 1525
target 5'  A    UUUU     G       C 3'
            GCUU    GCCCU C GUGAC
            CGAG    UGGGA G UACUG
miRNA  3' GA    UU       G U     A 5'   mfe: -25.0 kcal/mol
```

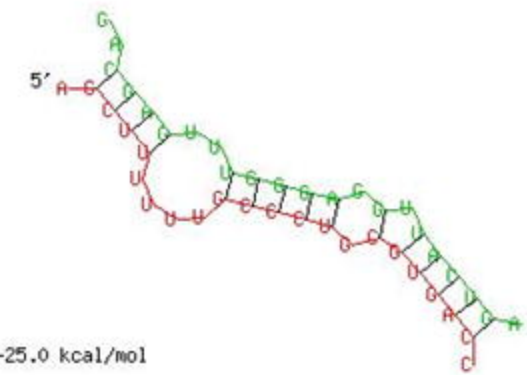


**C**

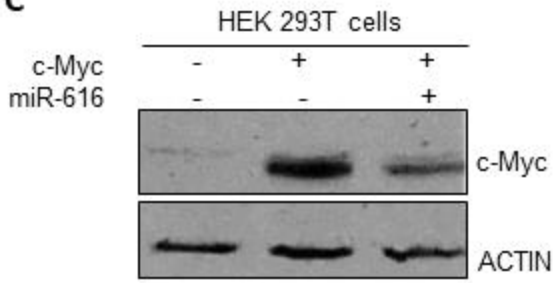


**D**

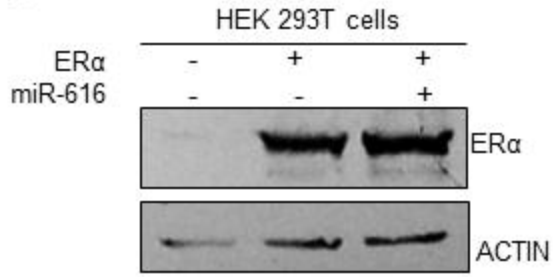


**E**

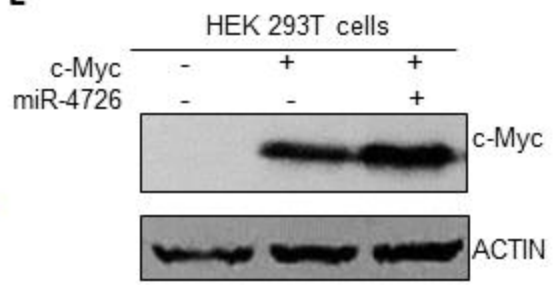


**Figure 8**

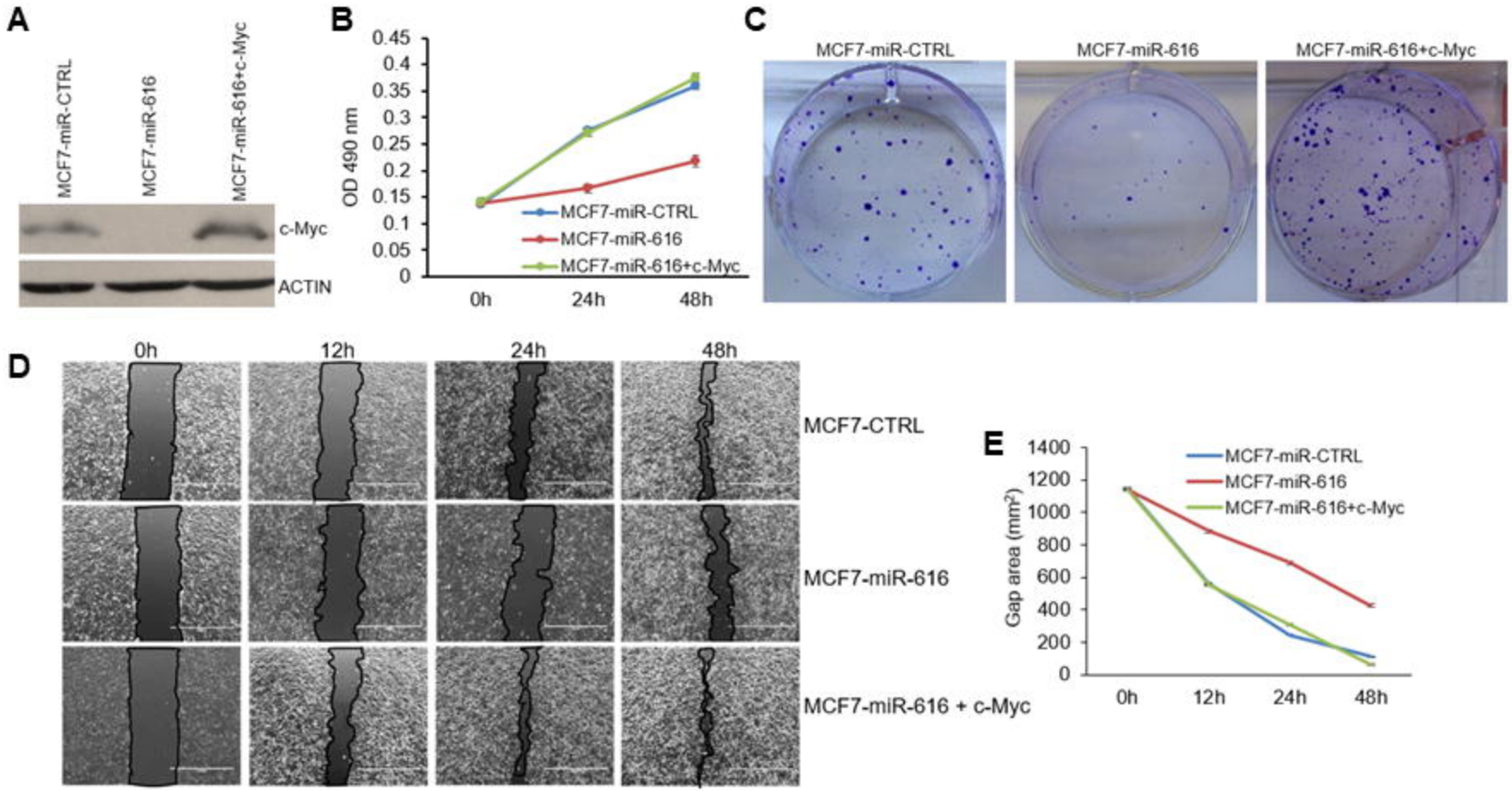
A
MCF7-miR-CTRL
MCF7-miR-616
MCF7-miR-616+c-Myc
c-Myc
ACTIN
B
OD 490 nm
0.45
0.4
0.35
0.3
0.25
0.2
0.15
0.1
0.05
0
0h
24h
48h
MCF7-miR-CTRL
MCF7-miR-616
MCF7-miR-616+c-Myc
C
MCF7-miR-CTRL
MCF7-miR-616
MCF7-miR-616+c-Myc
D
0h
12h
24h
48h
MCF7-CTRL
MCF7-miR-616
MCF7-miR-616 + c-Myc
E
Gap area (mm²)
1400
1200
1000
800
600
400
200
0
0h
12h
24h
48h
MCF7-miR-CTRL
MCF7-miR-616
MCF7-miR-616+c-Myc

**Figure 9**

A

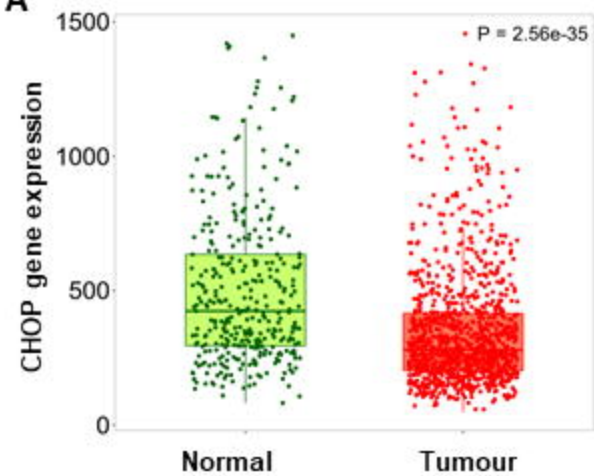


B

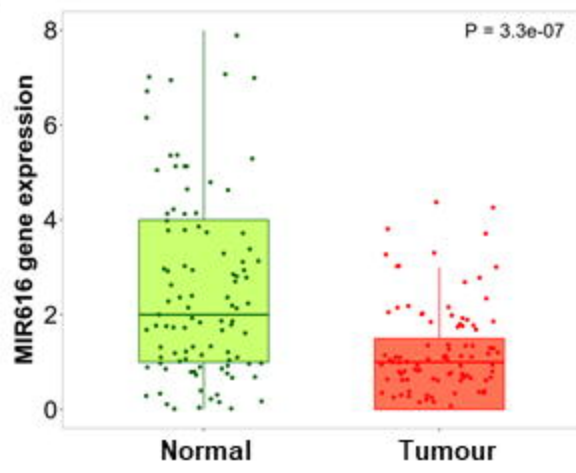


C

| Subtypes of breast cancer | Overall survival | |
|---|---|---|
| | Hazard Ratio | Logrank P |
| Luminal A | 1.57 (1.08 - 2.27) | **0.01600** |
| Luminal B | 0.81 (0.60 - 1.11) | 0.19000 |
| HER2 | 0.31 (0.16 - 0.61) | **0.00034** |
| TNBC | 0.75 (0.46 - 1.21) | 0.24000 |

**Figure 10**